

Change of Cr atoms distribution in Fe₈₅Cr₁₅ alloy caused by 250 keV He⁺ ion irradiation to different doses

S. M. Dubiel^{1*} and J. Żukrowski²

¹AGH University of Science and Technology, Faculty of Physics and Applied Computer Science, al. Adama Mickiewicza 30, 30-059 Kraków, Poland

²AGH University of Science and Technology, Academic Centre for Materials and Nanotechnology and Faculty of Physics and Applied Computer Science, al. Adama Mickiewicza 30, 30-059 Kraków, Poland

Redistribution of Cr atoms in a Fe₈₅Cr₁₅ alloy caused by its irradiation with 250 keV He⁺ ions to different doses, $D=8\cdot 10^{16}$, $16\cdot 10^{16}$ and $48\cdot 10^{16}$ ions/cm² was investigated by means of conversion electrons Mössbauer spectroscopy. The redistribution was expressed in terms of the Warren-Cowley short-range order parameters α_1 , α_2 and α_{12} pertaining to the first (1NN), second (2NN) and both i.e. 1NN+2NN shells, respectively. Clear evidence was found, both for non-irradiated and irradiated samples that the actual distribution of Cr atoms is characteristic of the shell, and for a given shell it depends on the irradiation dose. In particular, α_1 is positive, hence indicates an under population of Cr atoms in 1NN with respect to the random case, α_2 is negative, giving evidence thereby that 2NN is overpopulated by Cr atoms, and α_{12} is weakly positive. Under the applied irradiation the number of Cr atoms in both neighbor shells decreased signifying thereby a clustering of Cr atoms. The underlying decrease of Cr concentration within the 1NN-2NN volume around the probe Fe atoms was estimated at 1.5 at% ranging between 2.1 for the lowest and 0.8 at% for the highest dose.

Key words: ion irradiation, iron alloys, short-range ordering, micromagnetism, Mossbauer spectroscopy

*Corresponding author: Stanislaw.Dubiel@fis.agh.edu.pl

1. Introduction

Ferritic steels (FS) are manufactured based on Fe-Cr alloys. Their industrial and technological importance follows from their very good useful properties like swelling, high temperature corrosion and creep resistance [1,2]. Consequently, FS have been regarded as appropriate construction materials to be applied for the new generation of nuclear power facilities such as generation IV fission reactors and fusion reactors as well as for other technologically important plants like high power spallation targets [3–5]. In particular, they are used for a construction of such devices as fuel cladding, container of the spallation target or primary vessel. These devices work at service not only at elevated temperatures but also under irradiation conditions. In these circumstances, the materials undergo irradiation damage that can seriously deteriorate their mechanical properties. On the lattice scale, the radiation causes lattice defects, and, consequently, a redistribution of Fe/Cr atoms that can result in short-range order (SRO) or phase decomposition into Fe-rich and Cr-rich phases. Both these effects cause, among other, an enhancement of embrittlement. A better knowledge of the effect of irradiation on the useful properties of FS and underlying mechanisms is an important issue as it may be helpful in designing and fabrication of steels more resistant to the radiation damage, hence to extend the operational life of devices constructed therefrom. Fe–Cr alloys, that constitute the basic ingredient of FS, are often used as model alloys for investigations of both physical and materials properties [6 and references therein]. Here the effect of irradiation to different doses with $^4\text{He}^+$ ions of 250 keV on a model (EFDA/EURATOM) $\text{Fe}_{85}\text{Cr}_{15}$ alloy was studied with the conversion electrons Mössbauer spectroscopy (CEMS). The issue is of a practical importance, as a production of helium occurs during exposure of the devices to proton and/or neutron irradiation [1]. Its presence has a negative effect on the mechanical properties. In particular, it lowers the critical stress for intergranular structure and may induce a severe decrease of the fracture toughness [7]. Therefore, the understanding not only of the radiation damage but also of the effect of helium on the mechanical properties of FS is one of the important topics to be further studied.

2. Experimental

Samples investigated in this study were prepared from model EFDA/EURATOM master Fe₈₅Cr₁₅ alloy fabricated in 2007. It was delivered in the form of bar 10.9 mm in diameter, in a re-crystallized state after cold reduction of 70% and then heat-treated for 1h under pure argon flow at 850°C followed by air cooling. For the present study, a slice ~1 mm thick was cut off from the bar using a diamond saw, and it was subsequently cold-rolled (CR) down to a final thickness of ~25-30 μm. For the irradiation with 250 keV ⁴He⁺ ions at the JANNUS multi-ion beam irradiation platform at Centre National de la Recherche Scientifique, Saclay, France, samples in form of ~25 mm rectangles were used. They were irradiated to the dose of 8·10¹⁶, 16·10¹⁶ and 48·10¹⁶ ⁴He⁺·cm⁻² or 5, 10 and 30 dpa, respectively. The irradiation area had a diameter of 20 mm. An exemplary ion range and concentration profile is shown in

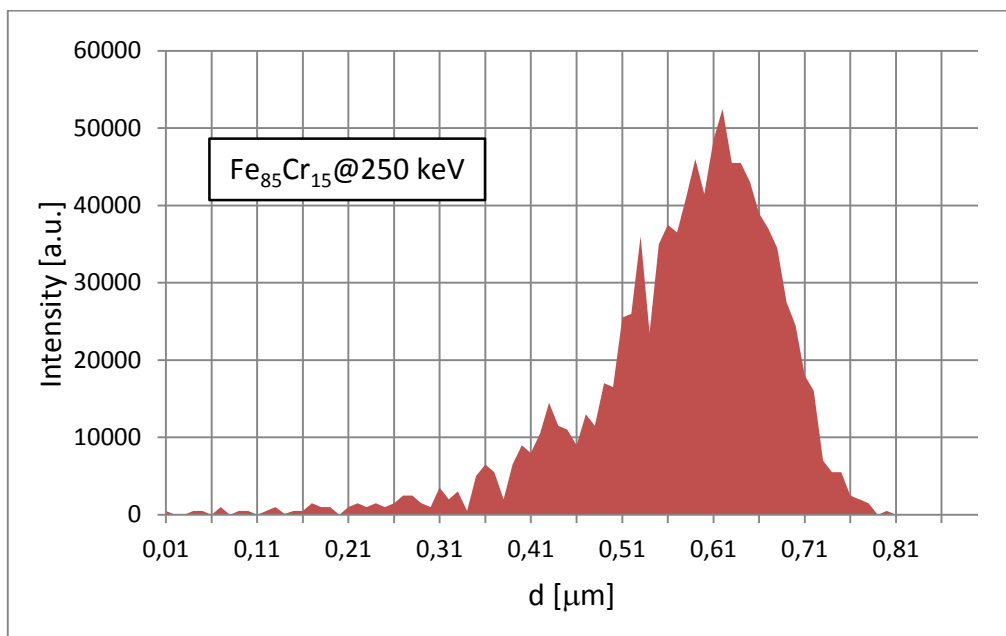


Fig. 1. He-concentration profile as measured for the Fe₈₅Cr₁₅ sample irradiated to the dose of 7.5 dpa with 250 keV He⁺. The range of ions is equal to 0.58 μm and the peak concentration ~10at%He.

⁵⁷Fe-site Mössbauer spectra were measured at room temperature (RT) recording conversion electrons (CEMS mode) in a backscattering geometry using a conventional constant acceleration spectrometer and a ⁵⁷Co(Rh) source of 14.4 keV gamma-rays with a nominal activity of 3.7 GBq. This means that they contain information concerning a pre surface layer

whose thickness is less than $\sim 0.3 \mu\text{m}$. Samples were placed in a proportional gas flow counter with a He/methane mixture as counting gas. The spectra recorded at room temperature both on the irradiated (IR) as well as on the non-irradiated (NIR) sides are displayed in Fig. 2. They were analyzed in terms of the two-shell model, assuming the effect of the presence of Cr atoms in the two-shells vicinity, 1NN-2NN, of the ^{57}Fe probe nuclei on the hyperfine field (B) and on the isomer is additive i.e. $X(n_1, n_2) = X(0, 0) + n_1 \cdot \Delta X_1 + n_2 \cdot \Delta X_2$, where $X = B$ or IS , ΔX_i is a change of B or IS due to one Cr atom situated in 1NN ($i=1$) or in 2NN ($i=2$). The number of Cr atoms in 1NN is indicated by n_1 , and that in 2NN by n_2 . Seventeen most probable atomic configurations, (n_1, n_2) , taken into account, were chosen based on the binomial distribution to fulfill the condition $\sum_{n_1, n_2} P(n_1, n_2) \geq 0.99$. However, their probabilities, $P(n_1, n_2)$, were treated in the fitting procedure as free parameters (their starting values were those from the binomial distribution). All spectral parameters like $X(0, 0)$, ΔX_i , line widths of individual sextets $G1$, $G2$ and $G3$ and their relative intensities (Clebsch-Gordan coefficients) $C2$ and $C3$ were treated as free ($C1=1$). Very good fits (in terms of χ^2) were obtained with the spectral parameters that are displayed in Table 1. Their values are in a very good agreement with the corresponding ones obtained previously for Fe-Cr alloys [8,9].

The knowledge of the atomic configurations, (n_1, n_2) , and their probabilities, $P(n_1, n_2)$, permitted to determine next the average number of Cr atoms in 1NN, $\langle n_1 \rangle = \sum_{n_1, n_2} n_1 P(n_1, n_2)$, in the

second, $\langle n_2 \rangle = \sum_{n_1, n_2} n_2 P(n_1, n_2)$ and in both shells, $\langle n_{12} \rangle = \sum_{n_1, n_2} (n_1 + n_2) P(n_1, n_2)$. The

knowledge of $\langle n_1 \rangle$, $\langle n_2 \rangle$, and $\langle n_{12} \rangle$, was next used, in turn, in order to calculate the corresponding SRO parameters, α_1 , α_2 , and α_{12} , as outlined below.

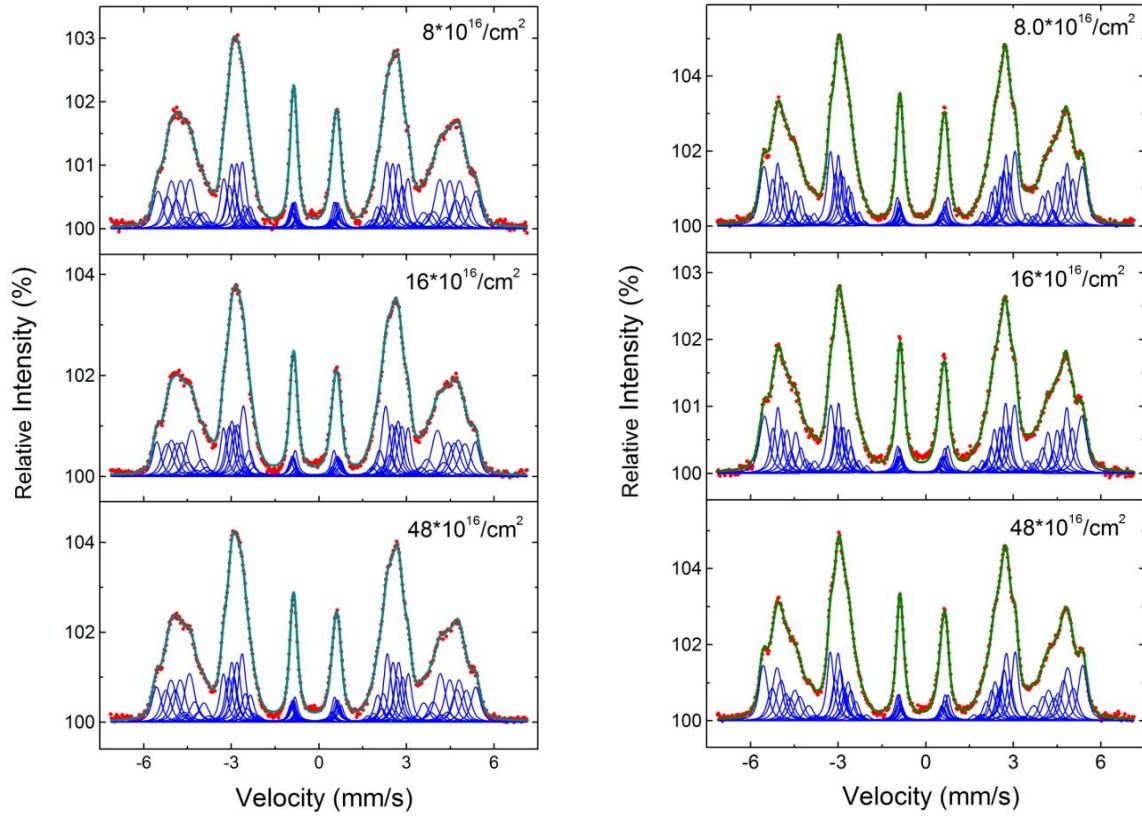


Fig. 2. ^{57}Fe Mössbauer spectra recorded at RT on the non-irradiated sides of the samples (left panel) and those recorded on the irradiated sides of them (right panel). Sub spectra corresponding to particular atomic configurations taken into account in the fitting procedure are indicated.

Table 1 Best-fit values of spectral parameters obtained from the spectra recorded on the non-irradiated (NIR) and irradiated (IR) sides. Meaning of the parameters is given in the text. The values of $IS(0,0)$ are relative to the source of the gamma rays.

Sample	Dose ($10^{16}/\text{cm}^2$)	$B(0,0)$ [T]	ΔB_1 [T]	ΔB_2 [T]	$IS(0,0)$ [mm/s]	ΔIS_1 [mm/s]	ΔIS_2 [mm/s]	G1/2 [mm/s]	G2/2 [mm/s]	G3/2 [mm/s]	C2/C3
$\text{Fe}_{85}\text{Cr}_{15}$ NIR- sides	8/NIR	33.45(1)	-2.95(8)	-1.94(7)	-.086(3)	-.016(6)	-.001(4)	.235(9)	.181(6)	.125(3)	3.1(1)
	16/NIR	33.57(5)	-3.1(1)	-2.06(6)	-.096(3)	-.021(7)	-.013(2)	.195(7)	.141(5)	.127(2)	3.3(1)
	48/NIR	33.71(8)	-3.3(1)	-1.97(6)	-.099(2)	-.024(1)	-.011(2)	.160(5)	.132(4)	.118(2)	3.4(1)
$\text{Fe}_{85}\text{Cr}_{15}$ IR-sides	8/IR	33.87(2)	-3.05(4)	-1.91(3)	-.096(2)	-.020(1)	-.015(2)	.162(4)	.128(3)	.120(2)	3.0(1)
	16/IR	33.60(4)	-3.18(3)	-2.13(2)	-.095(2)	-.025(2)	-.011(1)	.173(6)	.139(5)	.125(2)	3.0(1)
	48/IR	33.87(4)	-3.05(7)	-1.95(7)	-.096(1)	-.017(2)	-.010(2)	.162(4)	.136(3)	.119(2)	3.1(1)

3. Results and discussion

3.1. Short-range order (SRO) parameters

A distribution of Cr atoms in the iron matrix can be quantitatively described in terms of Warren-Cowley short-range order (SRO) parameters, α_i . The method applied in the present study i.e. the Mössbauer spectroscopy enables determination of the SRO-parameters for the first, α_1 , and for the second, α_2 , nearest-neighbor shells, separately. Knowing both of them, one can also calculate the SRO-parameter for both shells, α_{12} . The knowledge of the SRO-parameters makes it possible to discuss the distribution of atoms in terms of their ordering or clustering (anti clustering). The values of α_k ($k=1,2,12$) were calculated based on the following equation:

$$\alpha_k = 1 - \frac{\langle n_k \rangle}{\langle n_{ok} \rangle} \quad (1)$$

Where $\langle n_k \rangle$ is the actual number of Cr atoms in the k -th near-neighbor shell, while $\langle n_{ok} \rangle$ is the number of Cr atoms in the k -th near-neighbor shell calculated assuming their distribution is random i.e. $\langle n_{01} \rangle = 0.08x$, $\langle n_{02} \rangle = 0.06x$, and $\langle n_{01} + n_{02} \rangle = 0.14x$.

3.1.1. Non-irradiated (NIR) side

Based on the analysis of the spectra recorded on the NIR-sides of the IR-samples the SRO-parameters α_1 , α_2 and α_{12} were determined and they are displayed in Fig. 3.

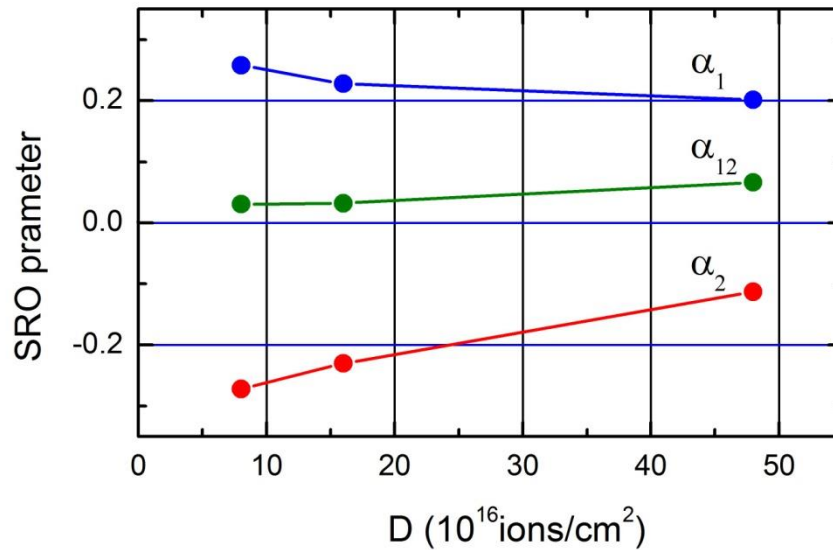


Fig. 3. SRO-parameters α_1 , α_2 and α_{12} determined from the CEMS spectra recorded on the NIR-sides of the IR-samples versus the irradiation dose, D . The solid lines are to guide the eye.

It follows from Fig. 3 that the SRO-parameters are characteristic of a given neighbour shell and, for a given shell, they depend on the irradiation dose, D . The values of α_1 are positive what implies that the number of Cr atoms in the 1NN-shell is lower than that expected for a random distribution. This can be interpreted as evidence that the interaction between Fe and Cr atoms being the nearest neighbor is repulsive. The amplitude of α_1 decreases with D . Contrary, α_2 has negative values indicating thereby that the number of Cr atoms in the 2NN shells is higher than that following from the binomial distribution. In other words, the interaction between Fe atoms and Cr atoms separated by the distance equal to the radius of the 2NN shell is attractive. The amplitude of α_2 linearly decreases with D . Values of α_{12} are weakly positive what mean that the number of Cr atoms within the 1NN-2NN volume around the probe Fe atoms is slightly lower than expected for a statistical distribution. Their number moderately increases with D .

3.1.2. Irradiated (IR) side

Evaluation of the spectra recorded on the IR-sides of the samples yielded the SRO-parameters that are illustrated in Fig. 4.

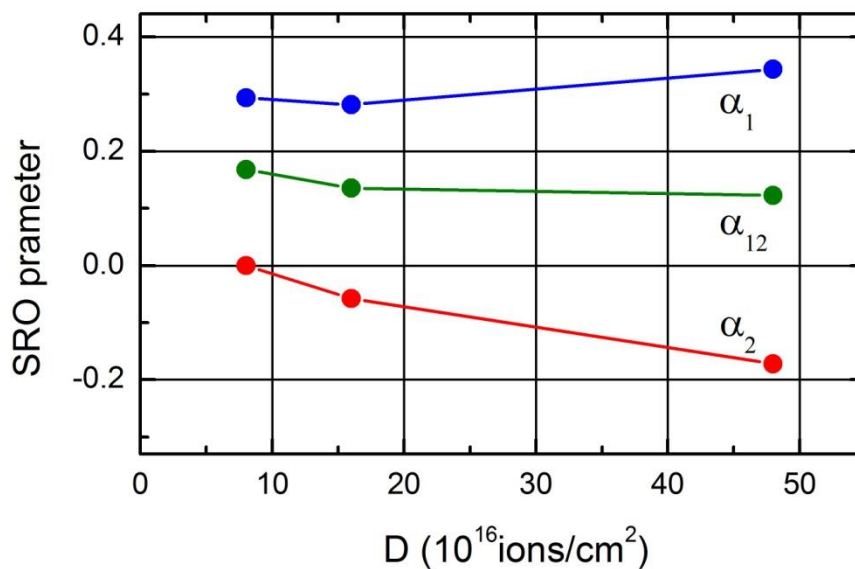


Fig. 4. SRO-parameters α_1 , α_2 and α_{12} determined from the CEMS spectra recorded on the IR-sides of the samples versus the irradiation dose, D . The solid lines are to guide the eye.

As in the case of the NIR-data, also in this case the SRO-parameters are characteristic of the neighbour shell. Those determined for 1NN are positive showing first a light decrease and then an increase with the dose; $\alpha_2 = 0$ for $D = 8 \cdot 10^{16}$ ions/cm² and it strongly decreases with D . Finally, α_{12} are positive for all irradiation doses but its amplitude shows a weak decrease with D . To reveal the real effect of the irradiation on the distribution of Cr atoms one has to take into account the initial distribution which was different. For that purpose a difference $\Delta\alpha_k = \alpha_k(\text{IR}) - \alpha_k(\text{NIR})$ ($k=1,2,12$) was calculated and presented in Fig. 5. It is clear that all three SRO-parameters are positive i.e. the number of Cr atoms in both neighbor shells had decreased under the applied irradiation. The biggest change in both shells is observed for the dose of $16 \cdot 10^{16}$ ions/cm² and the least one for $D = 8 \cdot 10^{16}$ ions/cm². However, the average change of the SRO-parameter in 1NN is greater than the one in 2NN (0.148 against 0.111). This behavior i.e. an increase of the values of the SRO-parameters upon irradiation means that the underlying redistribution of Cr atoms can be termed as irradiation-induced clustering.

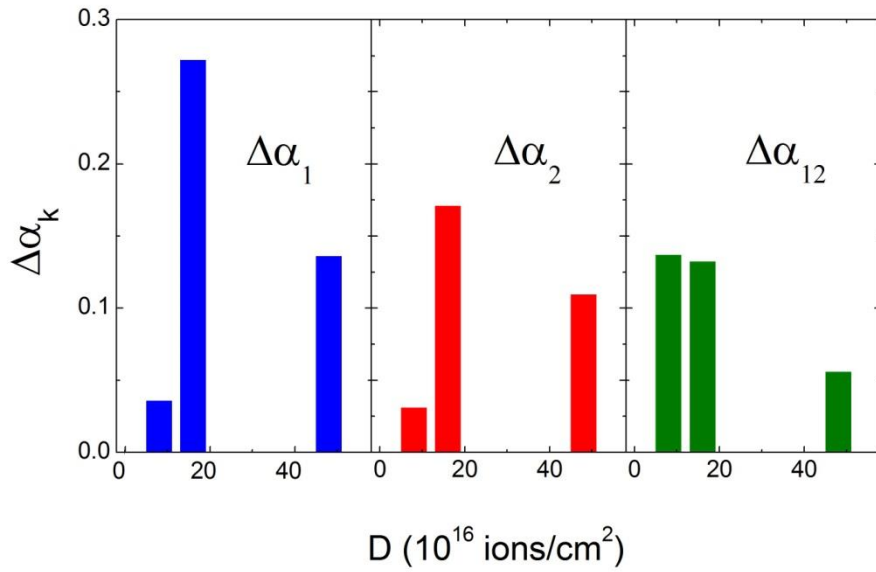


Fig. 5. Difference of the SRO-parameters $\Delta\alpha_k = \alpha_k(\text{IR}) - \alpha_k(\text{NIR})$ ($k=1,2,12$) as determined from the data shown in Figs. 3 and 4 versus the irradiation dose, D .

3.2. Local concentration change

An alternative way of describing the effect of the irradiation on the distribution of Cr atoms in the studied alloy is in terms of the underlying changes in the local Cr concentration. For that purpose we recalculate the average number of Cr atoms in 1NN shell, $\langle n_1 \rangle$, that in 2NN shell, $\langle n_2 \rangle$, as well as the one in 1NN-2NN shells, $\langle n_{12} \rangle$ into the concentration, x_k , by using the following equation:

$$x_k (\text{at}\%) = \frac{\langle n_k \rangle}{M} 100 \quad (2)$$

where $M=8, 6, 14$ for $k=1, 2, 12$, respectively.

Table 2. Concentration of chromium in the k -th neighbor shell, x_k , as calculated using eq. (2) for the non-irradiated (NIR) and irradiated (IR) sides of the samples. The dose of irradiation is indicated by D .

D		NIR			IR		
ions/cm ²	dpa	x_1	x_2	x_{12}	x_1	x_2	x_{12}
$8 \cdot 10^6$	5	11.25	19.3	14.7	10.7	15.15	12.6
$16 \cdot 10^6$	10	11.7	18.6	14.7	10.9	16.0	13.1
$48 \cdot 10^6$	30	12.1	16.9	14.15	9.95	17.75	13.3

From the data displayed in Table 2 it is evident that the concentration of Cr atoms both in NIR and in IR samples in the 1NN shell is lower than the value of 15.15 at% determined by chemical analysis and that in the 2NN shell it is higher. In the NIR samples the highest difference was found for the sample irradiated to the dose of $8 \cdot 10^{16}$ ions/cm² and the lowest one for the sample irradiated to the maximum dose. In the IR sample the situation is reversed: the strongest deviation from the chemically determined concentration was revealed for the sample irradiated to the highest dose, while in the sample irradiated to the smallest dose the deviation is minimal. The opposite relation is true as far as the concentration averaged over both shells, x_{12} , is concerned. In any case, the x_{12} -values determined for the IR samples are smaller, on average by 1.5 at%, than those found for the NIR-samples. This effect can be understood in terms of the clustering of Cr atoms.

3.3. Effect on the hyperfine field

Further evidence in favor of the irradiation-induced clustering of Cr atoms is shown in Fig.6. As shown the average hyperfine field, $\langle B \rangle$, is linearly correlated with the average number of Cr atoms within the 1NN-2NN volume around the probe Fe nuclei. The $\langle B \rangle$ -values determined for the IR-samples have significantly higher values than those calculated for the NIR-samples. The observed increase of $\langle B \rangle$ by ~ 9 kOe is equivalent, in the light of the $B(x)$ relationship [8], to a decrease of x by $\sim 3(1)$ at%. The latter agrees reasonably with the corresponding figure deduced in paragraph 3.2.

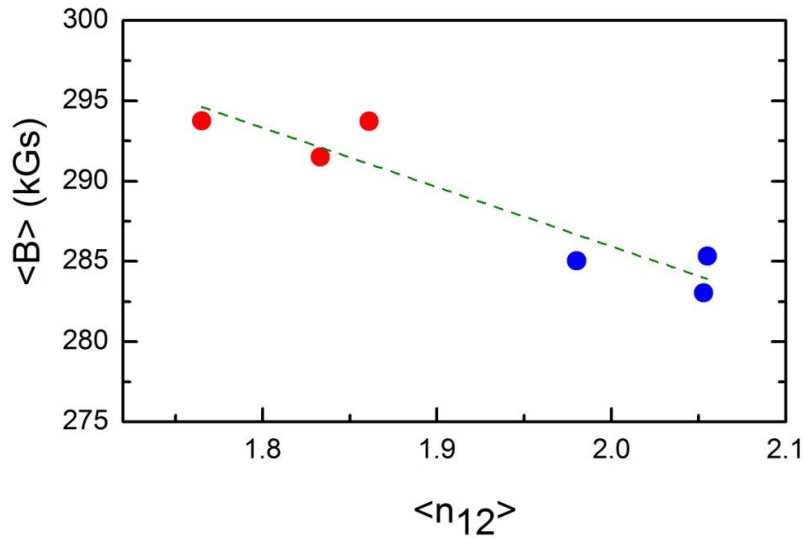


Fig. 6. Relationship between the average hyperfine field, $\langle B \rangle$, and the average number of Cr atoms in the 1NN-2NN shells, $\langle n_{12} \rangle$. The dashed line shows the linear fit to the data.

3.4. Effect on the magnetization vector

The knowledge of the Clebsch-Gordan coefficient C_2 permits determination of an angle between the direction of the γ -rays (in this case perpendicular to samples' surface) and that of the magnetization vector, Θ , based on the following equation:

$$C_2 = \frac{4 \sin^4 \Theta}{1 + \cos^2 \Theta} \quad (3)$$

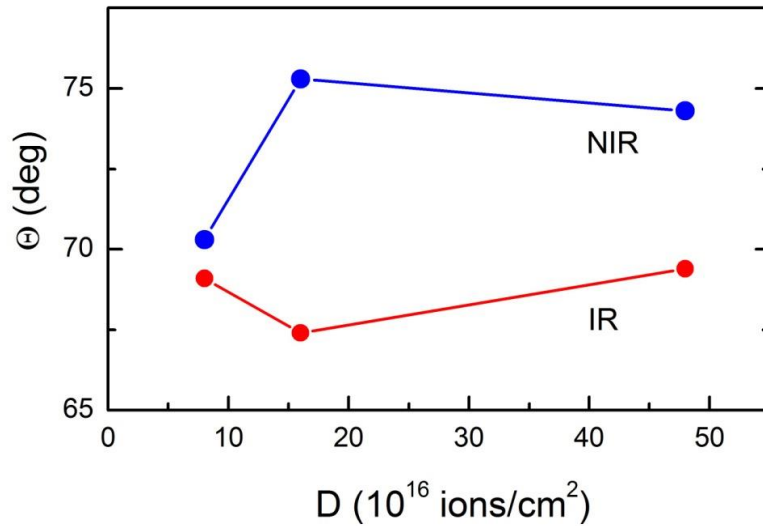


Fig. 7. Dependence of the angle Θ , on the dose of irradiation, D , for the non-irradiated (NIR) and irradiated (IR) sides of the investigates samples. The solid lines are a guide to the eye.

As illustrated in Fig. 7, the values of Θ in the irradiated samples are significantly smaller than those in the non-irradiated samples. It is also clear that in the NIR-samples Θ had different values reflecting thereby a lack of homogeneity as far as a cold-rolled-induced texture in the studied samples is concerned. Thus to reveal a genuine effect of the irradiation on Θ , a difference between Θ_{IR} and Θ_{NIR} , $\Delta\Theta$, was calculated and plotted in Fig. 8.

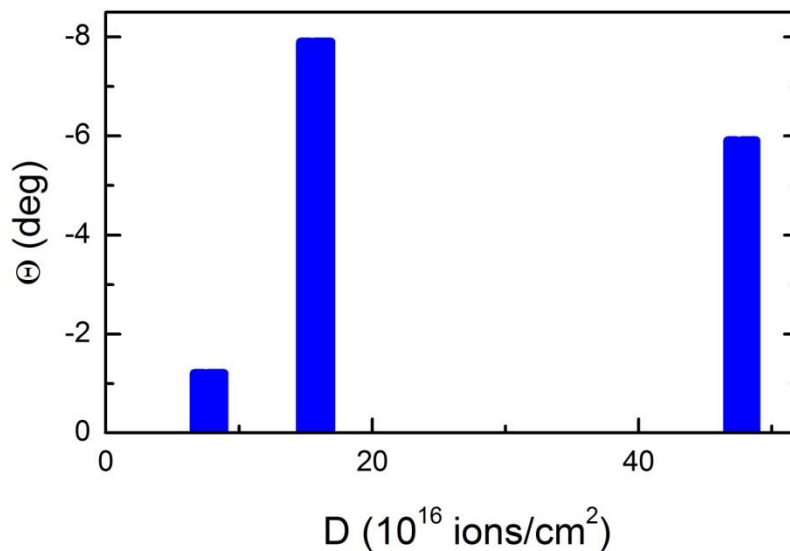


Fig.8. The difference in angle, $\Delta\Theta = \Theta_{IR} - \Theta_{NIR}$, for different doses of irradiation, D .

The data presented in Fig. 8 give evidence that Θ was different before the irradiation and it also depends on the irradiation dose. To account for the different initial values of Θ , a difference $\Delta\Theta = \Theta_{\text{IR}} - \Theta_{\text{NIR}}$ was calculated. The maximum decrease of Θ occurred for the sample irradiated to $D = 16 \cdot 10^{16}$ ions/cm² and the minimal one for the one irradiated to $8 \cdot 10^{16}$ ions/cm². The decrease of Θ upon irradiation of the Fe₈₅Cr₁₅ alloy with 25 keV He ions was already observed [10]. However, in that case the maximum change of Θ was $\sim 13^\circ$. The significantly higher rotation in the latter could have its origin in a much lower implantation range viz. 0.2 μm for 25 keV ions than that of 0.6 μm for 250 keV ions. Consequently, the rotation of the magnetization vector in the samples irradiated with 25 keV ions was due not only to a ballistic effect, as in the case of 250 keV ions, but also to a presence of He atoms in the pre surface layer accessible to CEMS measurements.

4. Conclusions

The results obtained in this study permit the following conclusions to be drawn:

1. The distribution of Cr atoms in a heavily deformed Fe₈₅Cr₁₅ alloy is not random: the nearest-neighbor shell is underpopulated ($\alpha_1 < 0$) while the second nearest-neighbor shell is overpopulated ($\alpha_2 > 0$) with Cr atoms.
2. The irradiation with 250 keV ⁴He⁺ ions caused redistribution of Cr atoms. Their number in both shells decreased: most significantly for the medium dose, and least significantly for the lowest dose.
3. The irradiation induced redistribution resulted in: (a) clustering of Cr atoms reducing thereby the local concentration of Cr atoms within the 1NN-2NN vicinity of Fe atoms by 1.5at%, (b) increase of the average hyperfine field by ~ 9 kOe, and (c) rotation of the magnetization vector towards the normal to the samples' surface by maximum of $\sim 8^\circ$ for the sample irradiated to the dose of $16 \cdot 10^{16}$ ions/cm.

Acknowledgement

This study was carried out within the IPPLM-EURATOM Association. It was also supported by The Ministry of Science and Higher Education, Warszawa, Poland. Mr. Yves Surreys is thanked for his expert assistance in the irradiation.

References

- [1] A. Hishinuma, A. Kohyama, R.L. Klueh, D.S. Gelles, W. Dietz, K. Ehrlich, J. Nucl. Mater. 258–263 (1998) 193
- [2] F.A. Garner, M.B. Toloczko, B.H. Sence, J. Nucl. Mater. 276 (2000) 123
- [3] L.K. Mansur, A.F. Rowcliffe, R.K. Nanstad, S.J. Zinkle, W.R. Corwin, R.E. Stoller, J. Nucl. Mater. 329–333 (2004) 166
- [4] L. Malerba, A. Caro, J. Wallenius, J. Nucl. Mater. 382 (2008) 112
- [5] K.H. Lo, C.H. Shek, J.K.L. Lai, Mater. Sci. Eng. R 65 (2009) 39
- [6] W. Xiong, M. Selleby, Q. Chen, J. Odqvist, Y. Du, Crit. Rev. Sol. State. Mater. Sci. 35 (2010) 125
- [7] Y. Dai, J. Henry, Z. Tong, X. Averty, J. Malaplate, B. Long, J. Nucl. Mater. 415 (2011) 306
- [8] S. M. Dubiel, J. Żukrowski, J. Magn. Magn. Mater., 23 (1981) 214
- [9] S. M. Dubiel, J. Żukrowski, Acta Mater., 61 (2013) 6207
- [10] S. M. Dubiel, J. Cieślak, H. Reuther, J. Nucl. Mater., 434 (2013) 235